PCCP

PAPER

View Article Online
View Journal | View Issue

Cite this: *Phys. Chem. Chem. Phys.*, 2026, **28**, 5161

CO_2, N_2 and H_2 adsorption in Zn^{2+}-containing zeolites and metal–organic frameworks

Pragnya Paramita Samal,[abc] Fabian Berger, †*[a] Sailaja Krishnamurty[bc] and Joachim Sauer [a]

Received 29th October 2025,
Accepted 16th January 2026

DOI: 10.1039/d5cp04169d

rsc.li/pccp

We employ a chemically accurate (±4 kJ mol^{-1}) embedding approach to calculate enthalpies for CO_2, N_2, and H_2 adsorption in the Zn^{2+}-containing zeolites FAU and CHA, and for CO_2 and H_2 in the metal–organic frameworks (MOFs) Zn-MOF-74 and CALF-20. Using MP2 as the high-level method and PBE+D4 as the periodic low-level method (MP2:PBE+D4), we obtain CO_2 adsorption enthalpies of −46, −34, and −36 kJ mol^{-1} for Zn-CHA, Zn-MOF-74, and CALF-20, respectively, all within chemical accuracy limits of the experimental values of −42, −30, and −39 kJ mol^{-1}. For CO_2 in Zn-FAU, where no experimental data exist, we provide an MP2:PBE+D4 prediction of −49 kJ mol^{-1}. For N_2, we predict MP2:PBE+D4 adsorption enthalpies of −41 and −39 kJ mol^{-1} in Zn-CHA and Zn-FAU, respectively. CO_2 adsorption is stronger in the zeolites than in the studied MOFs. Across all systems, CO_2 adsorption tends to be stronger than N_2 adsorption and both are largely favoured over H_2. We observe inconsistent accuracy of PBE+D4 for the two MOFs, despite their similar characteristics, underscoring the need for high-level approaches in predictive screening. Additionally, we conclude that Zn^{2+} cations with open coordination sites act as the primary binding sites and that these cations preferentially occupy 6-membered rings in zeolites.

1. Introduction

As the world transitions from fossil fuels to cleaner sources of energy, hydrogen is emerging as a promising candidate.[1] At present, it is mainly produced through steam reforming,[2] a process that involves separating CO_2 from H_2. The CO_2 adsorption characteristics are also important for carbon capture techniques such as pressure swing adsorption (PSA)[3] and direct air capture (DAC).[4–6] These applications typically rely on gas adsorption into porous solid sorbents with high adsorption capacity, selectivity, reusability, and stability.[7–10] Zeolites are a class of materials that has been extensively used over the last decades for gas storage and as molecular sieves, in addition to their importance in heterogeneous catalysis.[11–15] However, recent advances in CO_2 capture have focused on metal–organic frameworks (MOFs) due to their chemical versatility.[16–22]

Zeolites, such as faujasite (FAU) and chabazite (CHA) with low Si/Al ratios, *i.e.*, high Al concentrations, are viable materials for effective CO_2 capture.[23–27] Incorporating metal cations, which balance the negative charges introduced by aluminium substitution into the framework, is a promising route to enhance (selective) adsorption. Among these zeolites, Zn-exchanged CHA with high Si/Al ratios has shown CO_2 adsorption capacities comparable to zeolite 13X of the FAU type.[28] Additionally, Mg^{2+}, Ca^{2+}, and Zn^{2+} have been identified as the most effective cations for selective CO_2 adsorption in gas mixtures among a set of investigated extra-framework metal cations.[29] Further, the Zn^{2+}-containing MOF CALF-20 displayed CO_2 selectivity over N_2 and even over water,[30] both of which can be ubiquitous under practical operating conditions. For reversible physisorption, the ideal heat of adsorption lies between −30 and −60 kJ mol^{-1}.[16–20] However, despite extensive experimental and computational studies, reported adsorption enthalpies vary widely, leading to uncertainty in the understanding of the underlying mechanisms and the reliability of predictions for adsorption processes.[31–34]

Yet, in the quest for accelerating materials development for (selective) CO_2 adsorption, understanding and accurately predicting adsorption strength and selectivity remains a key challenge. The adsorption properties are primarily influenced by the structure of the porous framework and by the distribution, position, and type of defects, framework-substituted sites, and extra-framework species within the materials.[35–37] To assess the accuracy of simulations, it is crucial to validate commonly used, approximate methods such as density functional theory (DFT),

[a] *Institut für Chemie, Humboldt-Universität zu Berlin, Unter den Linden 6, 10099 Berlin, Germany. E-mail: fabian.berger@chemie.hu-berlin.de*
[b] *Physical and Material Chemistry Division, CSIR-National Chemical Laboratory, Pune 411008, India*
[c] *Academy of Scientific and Innovative Research (AcSIR), Ghaziabad, 201002, India*
† Present address: Yusuf Hamied Department of Chemistry, University of Cambridge, CB2 1EW Cambridge, United Kingdom.

through comparison to chemically accurate (±4 kJ mol^{-1}), yet more computationally demanding, methods like second-order Møller–Plesset perturbation theory (MP2),[38] or to experiments.

In this work, we achieve chemical accuracy for CO_2 and H_2 adsorption at Zn^{2+} sites in the medium-pore zeolite CHA, and the Zn^{2+}-containing MOFs MOF-74 and CALF-20. Additionally, we provide predictions for the CO_2 adsorption enthalpies in Zn-FAU and for N_2 adsorption in Zn-CHA and Zn-FAU, for which no experimental data are available. To go beyond standard DFT, we employ a hybrid high-level quantum mechanics (QM): low-level QM subtractive mechanical embedding approach.[39–43] This method combines DFT with periodic boundary conditions (pbc) using the Perdew–Burke–Ernzerhof (PBE)[44,45] functional, augmented with Grimme's D4 dispersion correction,[46,47] and MP2 as the high-level method (denoted MP2:PBE+D4). As we will show in this work, at this level, the calculated CO_2 adsorption enthalpies for Zn-CHA, CALF-20, and Zn-MOF-74 deviate from experimental values by only 4, 3, and 4 kJ mol^{-1}, respectively,[28,30,48] and the binding of CO_2 tends to be preferred over N_2, and both bind significantly stronger than H_2.

2. Systems and models

2.1. Zeolites and metal–organic frameworks

The systems investigated in this study include FAU, CHA, MOF-74, and CALF-20, chosen for their relevance to gas adsorption.[24,25,49–51] Zn^{2+} is selected as the extra-framework cation due to its ionic radius being similar to that of divalent alkaline earth metals such as Ca^{2+} and Mg^{2+}, as well as to that of Li^+, all of which are highly effective for CO_2 adsorption.[28,52] Moreover, Zn^{2+} offers higher coordinative flexibility[53] and binds more strongly with CO_2 due to higher Lewis acidity compared to Ca^{2+} and Mg^{2+} cations.[53,54] Furthermore, Zn^{2+} is more abundant and more affordable compared to Li^+, which is among the most used and best-performing cations for CO_2 adsorption,[24] rendering Zn^{2+} a promising candidate to enhance (selective) CO_2 capture. Additionally, Zn^{2+} sites, as found in different MOFs and enzymes, are also known to interact strongly with CO_2 molecules.[55,56]

The coordination environment of Zn^{2+} cations can vary across the investigated zeolites CHA and FAU, and even within the same framework, depending on the specific cation location. In CHA, the coordination of Zn^{2+} changes from a rather symmetric threefold coordination by framework oxygen atoms in six-membered rings (6MR) to a less symmetric threefold coordination in eight-membered rings (8MR), see Fig. 1(a). In FAU, Zn^{2+} similarly exhibits a symmetric, threefold coordination in 6MRs at sites I and II and a symmetric, but fourfold coordination at site III, see Fig. 1(b).

For MOF-74 and CALF-20, in contrast to the zeolites, Zn^{2+} cations are incorporated into the framework and are fivefold coordinated. In MOF-74, the Zn^{2+} coordination is square pyramidal (see Fig. 2), whereas in CALF-20, it is trigonal bipyramidal, as shown in Fig. 3. In the investigated MOFs, only one type of Zn^{2+} site exists in each framework, at variance with the investigated zeolites, which contain different adsorption sites.

2.2. Models

The supercells used for the large-pore zeolite FAU are based on the unit cell taken from the International Zeolite Association (IZA) database.[57] To compensate for the charge of the introduced extra framework metal cations, Li^+ or Zn^{2+}, one or two Al atoms are incorporated into the zeolite framework, which leads to Si/Al ratios of 23 or 47, respectively. The simulation cells of the medium-pore zeolite CHA are obtained by multiplying the cell taken from the IZA database.[57] The simulation cell contains two aluminium atoms, resulting in a Si/Al ratio of 17. Al atoms are distributed according to Löwenstein's rule.[58] The optimised cell parameters for both FAU and CHA are given in Table S1 in the Supplementary Information (SI). Our nomenclature adheres to the recommendations of the IZA database[57] and is explained in Section S1 in the SI. Our models are not aimed at representing the exact experimental Si/Al ratios. Rather, we create models that mimic the local environments likely present in the experimental Si/Al regimes. Models of Zn-MOF-74 and CALF-20 are derived from the Cambridge Crystal Database (CSD).[59] Our Zn-MOF-74 model is based on a Niggli-reduced rhombohedral unit cell containing six Zn^{2+} ions connected by three $(dobdc)^{4-}$ organic linkers, resulting in 54 atoms per simulation cell. The CALF-20 simulation cell consists of 44 atoms with four Zn^{2+} centers. For all systems, only one molecule of CO_2, N_2, or H_2 is considered per simulation cell to focus on the adsorbate–substrate interactions in the low-coverage regime.

3. Methods

We extend beyond the standard computational approach, which relies on DFT with pbc and dispersion (DFT-D), by adopting a QM:QM approach. We use DFT-D as the low-level method to compute the potential energy surface (PES) for the entire periodic structure, while employing MP2 as the high-level method for cluster models to locally describe the interactions between the adsorbed molecule and the nearby framework. Hybrid MP2:DFT-D provides chemical accuracy for alkane adsorption in zeolites,[38,60–64] while a small but noticeable additional correction from MP2 to CCSD(T) has been observed for systems with strong hydrogen bonds.[62,63] The MP2:DFT-D approach is used for single point calculations for the most stable DFT-optimised adsorption structures only.

3.1. Adsorption energies and enthalpies

We use DFT-D to obtain the enthalpy of adsorption (H_{ad}), which is given by

$$H_{ad} = E_{ad} + E_{ZPV} + E_{therm} - RT, \quad (1)$$

where E_{ad} corresponds to electronic adsorption energies, E_{ZPV} refers to contributions of zero-point vibrational energies, E_{therm} to thermal energy corrections, and R to the universal gas constant. The adsorption energy (E_{ad}) is defined as the difference between the energy of the framework loaded with the gas molecule (referred to as the adsorbed complex, E_{AS}), and the

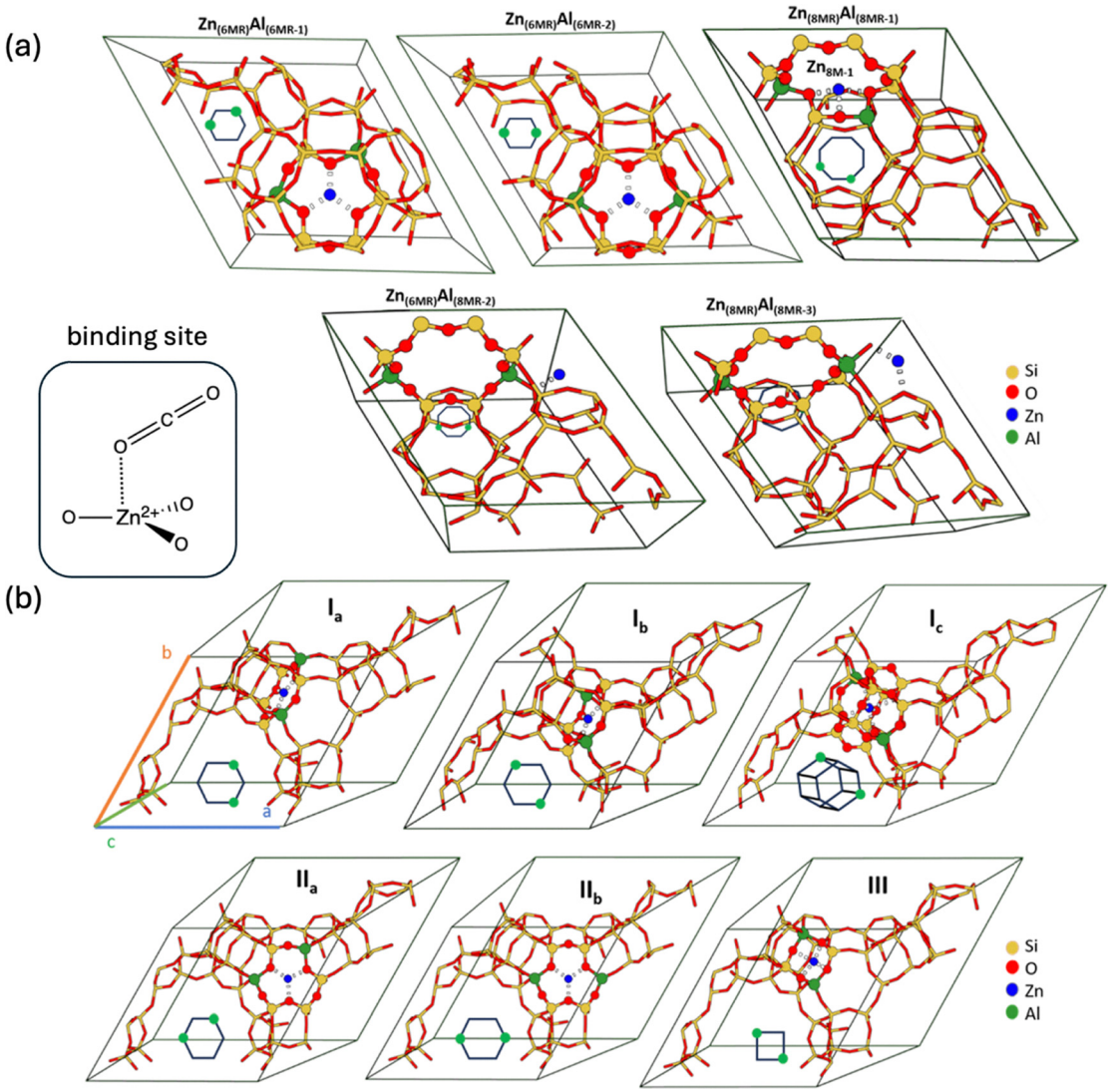

Fig. 1 Types of sites available in (a) CHA and (b) FAU for the location of extra framework cations, along with different Al distributions shown in 6MRs, 8MRs, and, in the case of FAU, for 4MRs. Dotted lines indicate attractive interactions between Zn^{2+} cations and adjacent framework oxygen atoms. The coordination environment of a Zn^{2+} cation binding to CO_2 is shown as well.

sum of energies of the gas molecule surrounded by vacuum (E_A) and the unloaded framework (E_S) within their relaxed structures,

$$E_{ad} = E_{AS} - (E_A + E_S). \quad (2)$$

3.2. Hybrid QM:QM calculations

For MP2:DFT-D calculations, the hybrid MP2:DFT-D electronic energy is defined as

$$E_{MP2}(S) \approx E_{MP2:DFT\text{-}D}(S, C) = E_{DFT\text{-}D}(S) + \Delta E_{HL}(C), \quad (3)$$

where $\Delta E_{HL}(C)$ is the high-level correction given by

$$\Delta E_{HL}(C) = E_{MP2}(C) - E_{DFT\text{-}D}(C). \quad (4)$$

$E_{MP2}(C)$ denotes the MP2 energy of a cluster model C, describing the adsorption site. $E_{DFT\text{-}D}(C)$ and $E_{DFT\text{-}D}(S)$ refer to the DFT-D energies of the same cluster model and the full periodic system, respectively. The MP2 quality adsorption enthalpy is then calculated as

$$H_{ad}(MP2) = E_{ad,MP2:DFT\text{-}D} + (E_{ZPV} + E_{therm})_{DFT\text{-}D} - RT. \quad (5)$$

The MP2:DFT-D adsorption energies are combined with the zero-point vibrational energy and thermal contributions calculated with DFT with pbc. Lastly, the Gibbs free energy of adsorption (G_{ad}) is calculated using:

$$G_{ad} = H_{ad} - T\Delta S_{ad}, \quad (6)$$

where T is the temperature, and ΔS_{ad} is the adsorption entropy.

3.3. Computational details

3.3.1. Density functional theory. DFT calculations employing the PBE functional,[44,45] augmented with Grimme's D2[46]

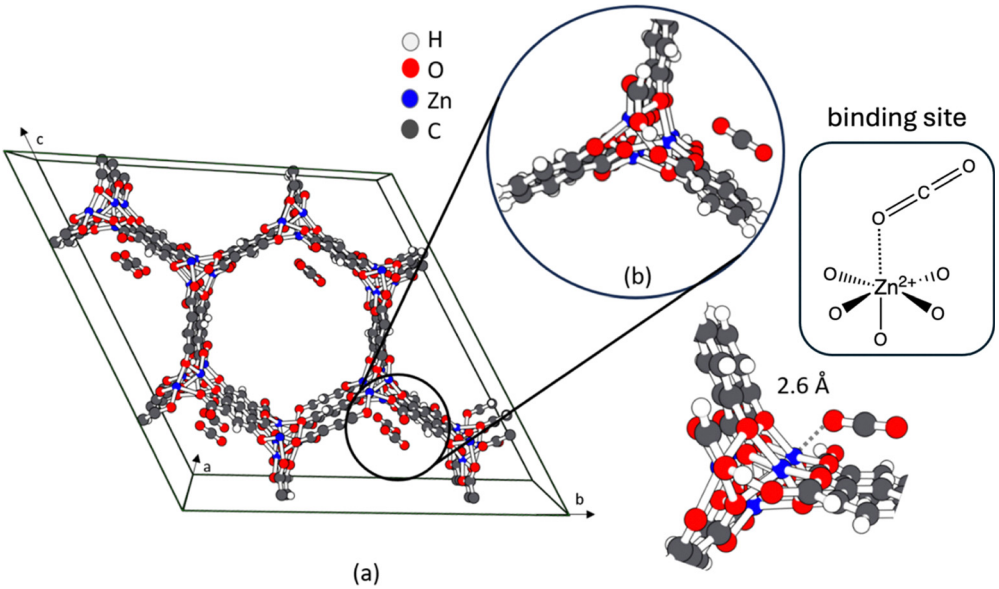

Fig. 2 (a) Periodic Zn-MOF-74 model, (b) cluster model for CO_2 adsorption. Cluster models are cut out of the periodic optimized structure of Zn-MOF-74 and used for MP2:PBE+D4 single point calculations. The dotted line indicates the shortest distance between a Zn^{2+} cation and an oxygen atom of the CO_2 molecule. The coordination environment of a Zn^{2+} cation binding to CO_2 is shown as well.

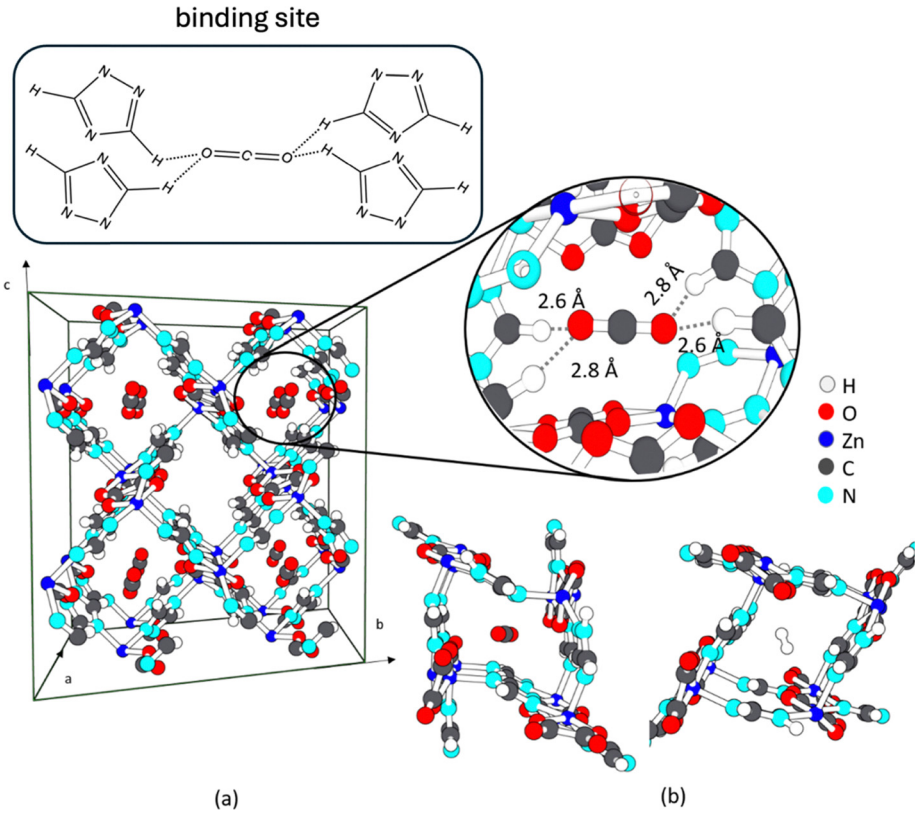

Fig. 3 (a) Periodic CALF-20 model, (b) cluster model for CO_2/H_2 adsorption. Cluster models are cut out of the periodic optimized structure of CALF-20 and used for MP2:PBE+D4 single point calculations. The dotted lines indicate the distances between framework hydrogen atoms and the oxygen atoms of the CO_2 molecule. The coordination environment of a Zn^{2+} cation binding to CO_2 is shown as well.

and D4[47] dispersion corrections, are conducted using the Vienna *ab initio* package (VASP)[65,66] version 5.4.1 and 6.2.1, respectively. These calculations make use of a plane-wave basis set for valence electrons, and the projector augmented wave

(PAW)[67] method for core electrons. Structure optimisations are performed with energy cutoffs of 400 eV (for FAU, CHA, and CALF-20) and 900 eV for MOF-74. Cell shape and size optimisations are performed using an energy cutoff of 800 eV to reduce the volume change effects on basis sets and are iterated until convergence is reached for all above-mentioned frameworks except MOF-74, for which 900 eV is used. The Brillouin zone is sampled at the Γ-point only. Convergence thresholds are set to 10^{-7} eV for electronic energy changes and 0.005 eV $Å^{-1}$ for structure optimisations. Stationary points are confirmed through a normal mode analysis by ensuring that no imaginary frequencies are observed. PBE+D2 and PBE+D4 numerical Hessians are computed using central finite differences with Cartesian displacements of 1 pm and an energy convergence threshold of 10^{-8} eV to determine harmonic zero-point vibrational energies and thermal enthalpy contributions, as well as entropies using the MonaLisa code.[40,68] The results obtained with PBE+D4 are reported in the main text, and for PBE+D2 in the SI.

3.3.2. Post-Hartree–Fock methods. Hybrid QM:QM calculations[39,41–43,69] employ a subtractive mechanical embedding scheme to achieve an MP2[70] quality PES using the MonaLisa code.[40,68] A cluster comprising the adsorbate and part of the framework in its vicinity is extracted from the periodic structure, ensuring a conservative distance of at least 10 Å around the CO_2, N_2, or H_2 molecules. For the cluster models of FAU, CHA, MOF-74, and CALF-20, the dangling bonds are saturated with H atoms as explained in Section S1 in the SI. The structures of the clusters are illustrated in Fig. 2 and 3, as well as S1 and S2 in the SI. Single point cluster calculations are corrected for the basis set superposition error (BSSE)[71] using the Counterpoise correction and carried out with the ORCA program,[72–74] version 5.03, employing the def2-TZVP[75–77] basis sets for PBE+D4 cluster calculations. Additionally, domain-based local pair natural orbital (DLPNO) MP2[78,79] energies are extrapolated to the complete basis set limit using a two-point extrapolation scheme[80,81] with cc-pV*X*Z basis sets (X = T, Q).[82,83] The 'TightPNO' and 'TightSCF' settings are applied. The term ''DLPNO'' is omitted hereafter for brevity. Example inputs are provided as part of the SI.

4. Results and discussions

4.1. Extra-framework cation location in the zeolites FAU and CHA

For FAU and CHA, we first examine the influence of the Al atom distribution in the zeolite frameworks on the preferred extra-framework cation locations. Different distributions of pairs of Al atoms in the framework are investigated for Zn^{2+} binding, as illustrated in Fig. 1(a) for CHA and in Fig. 1(b) for FAU. Tables S2 and S3 in the SI present the relative energies of Zn^{2+} and Li^+ binding to different sites in FAU.

For Zn^{2+}-containing CHA, X-ray diffraction (XRD), infrared (IR), and ultraviolet-visible (UV-vis) experiments[28] indicate that, depending on the synthesis, there are three distinct cation types: Zn^{2+}, $Zn(OH)^+$, and H^+. The trends for Zn^{2+}-containing CHA are presented in Table S4, while Tables S7 and S8 in the SI show the relative binding energies for $Zn(OH)^+$ and H^+.

For FAU, the trends for both cations (Li^+ and Zn^{2+}) are similar, with location at site II exhibiting the highest stability, followed by site I, and then site III. Cation adsorption at site III is least stable due to the strain induced by entering the small four-membered ring, in contrast to the more spacious six-membered rings of sites I and II. The higher stability of the Zn^{2+} cation at site II compared to site I may be attributed to its environment. Site II is located within a 6MR and opens into the larger 12MR. In contrast, site I, which is also situated in a 6MR, is confined within the sodalite cage of the FAU framework.

For CHA, Zn^{2+} cation adsorption in 6MRs is more stable than in 8MRs with a difference of more than 70 kJ mol^{-1} because, in 6MRs, the Zn^{2+} cation is symmetrically coordinated to three O atoms of the framework, exhibiting very similar bond distances from 1.95 to 1.98 Å, whereas, within 8MRs, Zn^{2+} is only directly bonded to one O atom with a distance of 1.97 Å. Even when two Al atoms are located in an 8MR, Zn^{2+} preferentially binds to a nearby 6MR. We denote such configurations as $Zn_{(6MR)}Al_{(8MR\text{-}2)}$, where the subscript on Zn indicates the ring in which the Zn^{2+} cation is located (here, a 6MR), and the subscript on Al denotes the ring containing the two Al atoms (here, an 8MR). The following number refers to the number of Si-containing T-sites separating the two Al atoms (in this case, 2). The binding energy for Zn^{2+} in this case is very similar to the case where Zn^{2+} is located in a 6MR with the two Al atoms located in the same 6MR, $Zn_{(6MR)}Al_{(6MR\text{-}2)}$. This suggests that for Zn^{2+} ions, the direct coordination environment, specifically the binding to framework oxygen atoms, plays a more important role than the proximity to framework Al atoms, which induce the negative charge in the framework. In contrast, for the protonated species, the proton is most stable when attached to an oxygen atom that is directly connected to an Al atom.

The relative energies for different locations of $Zn(OH)^+$ and protons in CHA are shown in Tables S7 and S8 in the SI, respectively. When $Zn(OH)^+$ is placed into a 6MRs, it is not stable and becomes protonated by the second Brønsted acid site (BAS), forming $Zn(OH_2)^{2+}$. Therefore, the formation of $Zn(OH)^+$ is only expected in high Si/Al samples without nearby excess protons that can form water coordinated to Zn^{2+}, or, if Al pairs are present in 8MRs of the CHA framework. This deviates from the preferred binding site of Zn^{2+} in 6MRs. Additionally, $Zn(OH)^+$ binding within 8MRs exhibits the highest stability in the configuration where two Al atoms are separated by two Si units in the same 8MR, $(Zn(OH)_{(8MR)}{}^+Al_{(8MR\text{-}2)})$. This configuration is more stable by 9 and 30 kJ mol^{-1} compared to $Zn(OH)^+$ in 8MR with two Al atoms separated by three Si units $(Zn(OH)_{(8MR)}{}^+Al_{(8M\text{-}3)})$ or one Si unit $(Zn(OH)_{(8MR)}{}^+Al_{(8M\text{-}1)})$, respectively.

For Zn^{2+}-containing CHA, our energy-based assignment of cation binding locations to framework oxygen atoms is corroborated by our calculated IR stretching frequencies, particularly around 850 and 916 cm^{-1} (reported in Table S4 in the SI). These frequencies, varying by 66 cm^{-1}, correspond to perturbed

T–O–T framework vibrations near the cations located within the 6MRs and 8MRs of CHA, respectively. The results might be considered consistent with experiments,[28] reporting IR stretching frequencies for T–O–T vibrations of 902 and 950 cm^{-1} for the 6MRs and 8MRs in CHA, respectively,[28] which differ by 48 cm^{-1}. Further, the bands are experimentally found to form in two stages,[28] which is consistent with our findings, suggesting that the 6MRs become populated by divalent Zn^{2+} cations before the 8MRs do so.

For extra-framework $Zn(OH)^+$ species, the calculated scaled harmonic IR frequency of the O–H stretching of $Zn(OH)^+$ located in 8MRs ranges from 3644 to 3675 cm^{-1} for different Al pair distributions, as shown in Table S7 in the SI. Following the literature,[84,85] the scaling approach is explained in Section S2 of the SI. When compared to the experimentally reported O–H stretching frequency for $Zn(OH)^+$ in CHA, 3665 cm^{-1},[28] our results are consistent with $Zn(OH)^+$ being located in 8MR and best agree for $Zn(OH)_{(8MR)}{}^{+}Al_{(8MR\text{-}2)}$, which we also predict to be the most stable adsorption site for $Zn(OH)^+$, see Table S7 in the SI.

4.2. CO_2, N_2, and H_2 adsorption

4.2.1. FAU and CHA zeolites. After having identified the most stable and thus most likely adsorption sites for the extra-framework species in the two zeolites FAU and CHA, we investigate the adsorption of CO_2, N_2, and H_2 at these Zn^{2+} sites. Table 1 presents the adsorption energies and enthalpies for CO_2, N_2, and H_2 adsorption on sites I, II, and III in Zn-FAU, calculated using PBE+D4. In Zn-FAU, site III exhibits the most exothermic adsorption of CO_2 and H_2, followed by sites I and II. However, as explained before, site III is the least stable Zn^{2+} location. Thus, the strong adsorption of −82 kJ mol^{-1} can be attributed to the low stability and thus higher reactivity of the Zn^{2+} in this location. While adsorption at site III is predicted to be strongest, the presence of this site in real samples is unlikely due to its instability, and therefore, it is not expected to contribute significantly to experimental observations. In contrast, site II, which is the preferred Zn^{2+} location, exhibits the weakest CO_2 adsorption of −48 kJ mol^{-1}, yet is expected to be most relevant in experimental samples.

Table 1 Calculated relative Zn^{2+} binding energies (E_{site}), adsorption energies (E_{ad}), and enthalpies (H_{ad}) at 298 K for CO_2, N_2, and H_2 adsorption in Zn-FAU (Si/Al = 23), obtained using PBE+D4. Also reported are zero-point energy corrections (ΔE_{ZPE}), thermal contributions (ΔE_{therm}), entropy contributions ($-T\Delta S_{ad}$), and relative Gibbs free energies (G_{ad}), all in kJ mol^{-1}, at a pressure of 0.1 MPa

Adsorbate	Site	E_{site}	E_{ad}	ΔE_{therm}	ΔE_{ZPV}	H_{ad}	$-T\Delta S_{ad}$	G_{ad}
CO_2	I_a	9	−64	1	5	−58	37	−21
	II_a	0	−48	−2	6	−44	43	−2
	III	128	−82	1	5	−76	49	−27
N_2	II_a	0	−38	−4	3	−39	43	4
H_2	I_a	9	−20	−4	7	−17	24	7
	II_a	0	−22	−4	8	−18	26	8
	III	128	−45	−5	9	−41	26	−15

In general, in agreement with literature,[29] the adsorption of CO_2 is stronger than that of N_2, and both are significantly stronger than H_2 adsorption, indicating that Zn-FAU preferentially adsorbs CO_2, then N_2, and only very weakly H_2. On site II, the adsorption enthalpy of CO_2 is −44 kJ mol^{-1}. N_2 adsorption is 5 kJ mol^{-1} less exothermic, −39 kJ mol^{-1}, and, for H_2, it is only −18 kJ mol^{-1}. Additionally, variations of as much as 20 to 40 kJ mol^{-1} occur for CO_2 and H_2 adsorption across different Zn^{2+} locations. The Gibbs free energies of CO_2 adsorption in Zn-FAU at all sites are negative, even though they reach −2 kJ mol^{-1} for site II, which is nearly thermoneutral. N_2 adsorption at site II is slightly endergonic, with a Gibbs free energy of adsorption of 4 kJ mol^{-1}. While CO_2 adsorption is exergonic across the framework, for H_2, only site III would allow spontaneous adsorption applying standard temperature and pressure. For comparison, adsorption energies and enthalpies calculated for CO_2 and H_2 on Zn^{2+} and Li^+ using PBE+D2 are reported in Tables S5 and S6 in the SI, and discrepancies of 2 to 10 kJ mol^{-1} are observed. Comparing both cations indicates that the adsorption trends are similar for sites I and II, but not for site III. At site III, adsorption energies obtained for Li^+ are weaker than for Zn^{2+}, which is attributed to the higher stability of the Li^+ cation at site III. This might be because in Li-FAU, only one Si is replaced by one Al, so site III is less strained in comparison to Zn-FAU, where two Al atoms replace two Si atoms.

We note that for weakly bound adsorbates, most notably H_2 in our study, our approach to computing adsorption enthalpies, entropies, and Gibbs free energies using a harmonic treatment around a single optimised configuration has inherent limitations. While a single optimised minimum provides a well-defined reference structure, weak adsorption corresponds to a shallow potential energy surface. Under such conditions, finite-temperature effects and anharmonicity may cause the adsorbate to sample multiple configurations or to diffuse into the pore rather than remain localized at a single binding site. For such cases, approaches based on molecular dynamics or Monte Carlo sampling would provide a more rigorous description of adsorption thermodynamics. In principle, adsorption enthalpies and free energies could be obtained from such simulations, ideally based on an MP2-quality potential energy surface. However, combining high-level electronic structure methods with extensive sampling would be computationally very demanding and is beyond the scope of the present work.

A proper finite-temperature description of weakly interacting alkanes in acidic zeolites has been achieved previously by some of us,[61] demonstrating that adsorption strengths are indeed reduced by a few kJ mol^{-1} when these effects are accounted for. Accordingly, the thermodynamic quantities reported here, which are based on the most stable binding motif, should be viewed as upper limits to the adsorption strength. Importantly, however, our calculated enthalpies for the more strongly binding CO_2 are in good agreement with experimental heats of adsorption, indicating that finite-temperature and anharmonic effects do not play a major role for CO_2. Moreover, these effects are expected to be least pronounced for the strongest adsorbate, CO_2, and most

Table 2 Calculated Zn^{2+} binding energies (E_{site}), adsorption energies (E_{ad}), and enthalpies (H_{ad}) at 298 K for CO_2, N_2, and H_2 adsorption in Zn-CHA (Si/Al = 17), obtained using PBE+D4. Also reported are zero-point energy corrections (ΔE_{ZPE}), thermal contributions (ΔE_{therm}), entropy contributions ($-T\Delta S_{ad}$), and relative Gibbs free energies (G_{ad}), all in kJ mol^{-1}, at a pressure of 0.1 MPa. Scaled PBE+D4 wavenumbers of CO_2 asymmetric stretching vibrations (ν_{CO_2}) and non-scaled stretching frequencies of T–O–T vibrations are given in cm^{-1}

Adsorbate	Site	E_{site}	E_{ad}	ΔE_{therm}	ΔE_{ZPV}	H_{ad}	$-T\Delta S_{ad}$	G_{ad}	ν_{T-O-T}	ν_{CO_2}
CO_2	$Zn_{(6MR)}Al_{(6MR-1)}$	10	−56	−1	6	−51	41	−10	837	2352[a]
	$Zn_{(6MR)}Al_{(6MR-2)}$	0	−56	−1	6	−51	42	−9	850	2357[a]
									902[b]	2356[b]
	$Zn_{(8MR)}Al_{(8MR-1)}$	84	−20	−4	10	−14	58	44	845	2348[a]
	$Zn_{(6MR)}Al_{(8MR-2)}$	1	−56	−1	6	−50	43	−7	916	2351[a]
									950[b]	
	$Zn_{(8MR)}Al_{(8MR-3)}$	76	−63	−1	6	−58	42	−16	900	2353[a]
N_2	$Zn_{(6MR)}Al_{(6MR-2)}$	0	−41	−3	3	−41	35	−6		
H_2	$Zn_{(6MR)}Al_{(6MR-1)}$	10	−20	−4	7	−17	24	7		
	$Zn_{(6MR)}Al_{(6MR-2)}$	0	−22	−4	8	−18	26	8		
	$Zn_{(8MR)}Al_{(8MR-1)}$	84	−18	−7	13	−12	31	19		
	$Zn_{(8MR)}Al_{(8MR-2)}$	1	−22	−4	8	−18	26	8		
	$Zn_{(8MR)}Al_{(8MR-3)}$	76	−25	−5	8	−22	27	5		

[a] Scaling factor = 0.9928 as explained in the scaling approach in Section S2 in the SI. [b] Experimental values taken from ref. 28.

pronounced for the weakest one, H_2, which would further increase the energetic separation between adsorption of CO_2 or N_2 and H_2 adsorption. Consequently, our harmonic calculations provide a conservative estimate of the selectivity among the three adsorbates.

For the CHA framework, Table 2, as well as S7 and S8 in the SI, present the adsorption energies and enthalpies calculated using PBE+D4. To fully understand CO_2 adsorption in these Zn-CHA samples, all three potentially occurring cation types are investigated. The adsorption energies and enthalpies for CO_2 and H_2 adsorbed at all sites, including small (6MRs) and large intersections (8MRs) are exothermic. For the Zn^{2+} cation, the calculated adsorption enthalpy of CO_2 for $Zn_{(6MR)}Al_{(6MR-2)}$ and $Zn_{(6MR)}Al_{(8MR-2)}$ are −51 and −50 kJ mol^{-1}, respectively. While experiments yield a value of −42 kJ mol^{-1},[28] we will later show that this discrepancy is resolved by using the chemically accurate MP2:PBE+D4 approach. Adsorption enthalpies for CO_2 obtained with other dispersion methods, PBE+TS/HI[86–88] and PBE+MBD,[89] are −42 and −49 kJ mol^{-1}, respectively, with the former closely matching the experimentally observed adsorption enthalpy, which is in line with literature.[28] Therefore, these findings further suggest that PBE+TS/HI may be used as the preferred generalized gradient approximation (GGA) functional and dispersion combination in future studies of CO_2 interacting with metal cations in zeolites and other porous materials.

As for the assignment of preferred cation locations, we now calculate C═O stretching vibrations to validate the sites for CO_2 adsorption present in the experimental samples. To do so, we calculate spectroscopic signatures for CO_2 adsorbed at different sites and compare them to experimentally measured IR frequencies.[28] The calculated and scaled antisymmetric IR stretching frequencies of CO_2 adsorbed on Zn^{2+} cations located in 6MRs and 8MRs are in a very narrow range from 2348 to 2357 cm^{-1}. A CO_2 molecule being adsorbed on a Zn^{2+} cation in a 6MR (2357 cm^{-1}) most closely aligns with the experimentally observed frequency of 2356 cm^{-1},[28] which they also assign to CO_2 adsorption at a Zn^{2+} located in a 6MR. However, due to the narrow range of only 9 cm^{-1} for the calculated IR frequencies, an unambiguous assignment of the Zn^{2+} cation location is not possible solely based on this comparison. While the IR spectra might not allow for unambiguous assignment, our chemically accurate calculations for adsorption enthalpies are also in best agreement with experiments when Zn^{2+} is in the 6MRs of CHA. Additionally, our calculations indicate that Zn^{2+} is energetically most stable in 6MRs. Together, these findings provide compelling evidence for the prevalence of Zn^{2+} located in 6MRs in experimental samples.

Similar to FAU, CO_2 adsorbs more strongly than N_2, and both are strongly favoured over H_2 in cation-exchanged CHA.[90] In the present work, in all sites, there is at least a difference of 20 kJ mol^{-1} in the adsorption enthalpy between CO_2 and H_2 molecules, except for the $Zn_{(8MR)}Al_{(8M-1)}$ site, at which the difference is only 2 kJ mol^{-1}. This site, however, is the least stable and will most likely not occur. Consequently, ions located in the 6MRs and 8MRs exhibit selectivity towards CO_2 adsorption over H_2. N_2 adsorption lies energetically between CO_2 and H_2. It is around 10 kJ mol^{-1} weaker than CO_2 adsorption, but about 10 kJ mol^{-1} stronger than H_2 adsorption. The same order is retained in the Gibbs free energies of adsorption, which are −10 and −6 kJ mol^{-1} for CO_2 and N_2, respectively, whereas H_2 adsorption remains endergonic with a positive free energy of +8 kJ mol^{-1}. These results suggest that even in a nitrogen-containing atmosphere, CO_2 will preferentially adsorb at Zn^{2+} sites in zeolite CHA.

For $Zn(OH)^+$ in CHA, Table S7 in the SI shows the heats of adsorption for CO_2, which fall within the range of −38 to −43 kJ mol^{-1}. The adsorption is weaker at most of these sites compared to Zn^{2+} sites. This can be attributed to the reduced accessibility of Zn^{2+} cations in $Zn(OH)^+$ compared to bare Zn^{2+}, which is reflected in the distances between Zn^{2+} and CO_2. The Zn–(O═C═O) distance in $Zn(OH)^+$ is 3.0 Å, and thus

significantly longer than the corresponding distance in Zn^{2+}-containing CHA, which is only 2.2 Å. As $Zn(OH)^+$ only resides in 8MRs, CO_2 interacting with such species is also located in 8MR, which is consistent with experimental findings.[28,91]

To provide a complete picture of the adsorption process, our calculations suggest, in accordance with the literature,[28] that adsorption of CO_2 occurs first at Zn^{2+} sites, which are preferably located in 6MRs. Only when all these sites are occupied, CO_2 starts interacting with $Zn(OH)^+$ sites that are located in 8MRs. Table S8 in the SI presents the adsorption enthalpies of CO_2 in CHA and compares adsorption at all three cationic species (Zn^{2+}, $Zn(OH)^+$, and H^+). Adsorption of CO_2 at the most stable BAS sites is weaker than at the most stable Zn^{2+} and $Zn(OH)^+$ sites by 13 (6MR) and 14 kJ mol^{-1} (8MR), respectively. These findings imply that CHA with a higher number of Zn^{2+} cations in 6MRs is desirable for increasing the CO_2 adsorption capacity, and that the formation of $Zn(OH)^+$ species and BASs should be minimised for gas adsorption and separation purposes.

4.2.2. Zn-based MOFs (Zn-MOF-74 and CALF-20). To explore the interaction of CO_2 and H_2 with Zn^{2+} as a framework cation in different MOFs, we investigate Zn-MOF-74 and CALF-20. These frameworks are chosen due to their industrial importance for CO_2 capture from the flue gas post-combustion process.[30,92–99] Fig. 2 and 3 show the optimised structures for Zn-MOF-74 and CALF-20, respectively. The calculated adsorption characteristics for Zn-MOF-74 and CALF-20 are given in Table 3. In the case of Zn-MOF-74, using PBE+D4, the adsorption energies obtained for CO_2 and H_2 are −27 and −7 kJ mol^{-1}, and the corresponding adsorption enthalpies for CO_2 and H_2 are −19 and −3 kJ mol^{-1}, respectively. The experimental adsorption enthalpies for CO_2 are −30 and −9 kJ mol^{-1} for H_2.[100–102] This reveals an 11 kJ mol^{-1} underestimation of the experimental enthalpy by PBE+D4 for CO_2 adsorption and of 6 kJ mol^{-1} for H_2. Conversely, in CALF-20, the computed adsorption energy for CO_2 is −45 kJ mol^{-1} and the enthalpy is −37 kJ mol^{-1}, closely aligning with the experimental adsorption enthalpy of −39 kJ mol^{-1}.[30]

The experimental and calculated adsorption enthalpies suggest that the adsorption of CO_2 is stronger in CALF-20 than in MOF-74. There are several potential reasons for the difference in adsorption enthalpies. The pore size of Zn-MOF-74 is much bigger (8.58 Å)[103] than that of CALF-20 (4.3 Å)[51] which hints at the role of dispersion interactions. CALF-20 exhibits a dispersion contribution to the PBE+D4 adsorption energy for CO_2 of −38 kJ mol^{-1} (84% of total adsorption energy), which is substantially larger than the −13 kJ mol^{-1} (48% of total adsorption energy) obtained for Zn-MOF-74. This difference in contributions to the adsorption energy might explain the strongly varying accuracy of the used DFT functional when compared to experiments.

Even though the Zn^{2+} cation is more accessible in Zn-MOF-74 and CO_2 can interact more directly with the cation (as shown in Fig. 2, Zn–(O═C═O) bond distance is 2.6 Å), than in CALF-20 (as shown in Fig. 3, Zn–(O═C═O) distance is 3 Å), the better fit and tighter confinement in the latter framework, result in a stronger adsorption. The enhanced adsorption in CALF-20 is primarily governed by dispersion, rather than direct interactions between CO_2 and the Zn^{2+} sites.[104–106] Additionally, for CALF-20, the adsorption structure shows that the oxygen atoms of the CO_2 molecule form weak hydrogen bonds with the framework hydrogen atoms (see Fig. 3(a)), which is not the case for MOF-74.

The Gibbs free energies for CO_2 and H_2 adsorption in both MOFs are positive, suggesting that adsorption is thermodynamically unfavourable under standard conditions. Therefore, either increasing the pressure or lowering the temperature is required to promote adsorption. Furthermore, when comparing the investigated MOFs with the zeolites, the Zn-based MOFs exhibit weaker adsorption strengths.

4.3. MP2 quality adsorption enthalpies and comparison to experiment

Overall, the PBE+D4 adsorption enthalpies deviate from the experimental heats of adsorption by up to 11 kJ mol^{-1}. This suggests that adsorption is already fairly well described with DFT in the investigated materials. Still, a significant improvement is observed with the hybrid MP2:PBE+D4 approach. Fig. 2 and 3, as well as S1 and S2 in the SI, show the cluster models used for the QM:QM calculations, with details described in Section S1 in the SI. The adsorption energies, enthalpies, and Gibbs free energies obtained for CO_2, N_2 and H_2 using the hybrid MP2:PBE+D4 approach are shown in Table 4.

The MP2:PBE+D4 adsorption enthalpies align with the PBE+D4 trend in adsorption strength: CO_2 adsorbs most strongly, followed by N_2, with H_2 binding most weakly. However, the MP2:PBE+D4 Gibbs free energies of adsorption, which ultimately determine adsorption equilibria, alter this ordering in Zn-CHA. In this zeolite, N_2 adsorption (−7 kJ mol^{-1}) becomes more exergonic than CO_2 adsorption (−4 kJ mol^{-1}). From the perspective of selective CO_2 adsorption and carbon capture applications, preferential N_2 adsorption is undesirable in nitrogen-containing environments. In contrast, for Zn-FAU the MP2:PBE+D4 Gibbs free energies predict exergonic CO_2 adsorption (−6 kJ mol^{-1}), while adsorption of N_2 and H_2 is endergonic, with values of 2 and 12 kJ mol^{-1}, respectively. This indicates that Zn-FAU is a promising material for selective CO_2 separation, not only from H_2 but also in N_2-containing atmospheres.

Comparison with experiment shows that for Zn-CHA, the CO_2 adsorption enthalpy calculated using PBE+D4 is

Table 3 Calculated adsorption energies (E_{ad}) and enthalpies (H_{ad}) at 298 K for CO_2 and H_2 adsorption in Zn-MOF-74 and CALF-20, obtained using PBE+D4. Also reported are zero-point energy corrections (ΔE_{ZPE}), thermal contributions (ΔE_{therm}), entropy contributions ($-T\Delta S_{ad}$), and relative Gibbs free energies (G_{ad}), all in kJ mol^{-1}, at a pressure of 0.1 MPa

Framework	Adsorbate	E_{ad}	ΔE_{therm}	ΔE_{ZPV}	H_{ad}	$-T\Delta S_{ad}$	G_{ad}
Zn-MOF-74	CO_2	−27	2	6	−19	29	10
	H_2	−7	−1	5	−3	16	13
CALF-20	CO_2	−45	2	6	−37	46	9
	H_2	−13	−2	6	−9	23	14

Table 4 Calculated adsorption energies (E_{ad}^{MP2}), enthalpies (H_{ad}^{MP2}), and relative Gibbs free energies (G_{ad}^{MP2}), all in kJ mol^{-1}, at a pressure of 0.1 MPa at 298 K for CO_2, N_2, and H_2 adsorption in Zn-FAU, Zn-CHA, Zn-MOF-74, and CALF-20 as obtained with MP2:PBE+D4. Adsorption enthalpies (H_{ad}^{PBE+D4}) calculated with PBE+D4 and experimental enthalpies (H_{ad}^{exp}) are also shown

Adsorbate	Framework	Site	H_{ad}^{exp}	H_{ad}^{PBE+D4}	E_{ad}^{MP2}	H_{ad}^{MP2}	G_{ad}^{MP2}
CO_2	CHA	II[a]	−42	−51	−51	−46	−4
	FAU	I_a		−58	−62	−56	−19
	FAU	II_a		−44	−53	−49	−6
	MOF-74	—	−30	−19	−42	−34	−5
	CALF-20	—	−39	−37	−43	−36	10
N_2	CHA	II[a]		−41	−42	−42	−7
	FAU	II_a		−39	−40	−41	2
H_2	CHA	II[a]		−18	−19	−15	11
	FAU	I_a		−20	−16	−13	11
		II_a		−18	−18	−14	12
	MOF-74	—	−9	−7	−9	−5	11
	CALF-20	—		−13	−7	−3	20

[a] $Zn_{(6MR)}Al_{(6MR-2)}$.

−51 kJ mol^{-1}, while MP2:PBE+D4 yields a value of −46 kJ mol^{-1}, which is within chemical accuracy limits to the experimental measurement of −42 kJ mol^{-1}. For Zn-MOF-74, PBE+D4 predicts a CO_2 adsorption enthalpy of −19 kJ mol^{-1} with a substantially larger high-level correction of −15 kJ mol^{-1}, yielding an MP2:PBE+D4 value of −34 kJ mol^{-1}, which, again, is within chemical accuracy limits to the experimental result of −30 kJ mol^{-1}. In contrast, for CALF-20, the PBE+D4 adsorption enthalpy for CO_2 is −37 kJ mol^{-1} and already very close to the MP2:PBE+D4 value of −36 kJ mol^{-1}. Both values are in excellent agreement with the experimental result of −39 kJ mol^{-1}. This shows that for CALF-20, PBE+D4 provides good agreement with experiments, whereas it performs much worse for MOF-74, highlighting that even for seemingly similar systems (Zn-containing MOFs) and the same adsorbate (CO_2), DFT can exhibit inconsistent performance and can be inaccurate when compared to experiments. In contrast, MP2:PBE+D4 not only yields chemically accurate adsorption enthalpies, but it does so reliably and consistently for all systems.

The observed energy differences between the PBE+D4 and MP2:PBE+D4 approaches can be attributed to MP2's more accurate treatment of dispersion interactions and metal–CO_2 interactions. The inconsistent discrepancies between DFT predictions and experimental values, as well as the varying high-level (HL) corrections, suggest that the nature of CO_2 adsorption differs across the MOFs. This is further supported by the differing contributions of dispersion to the PBE+D4 adsorption energies. These findings underscore the limitations of commonly used DFT methods and the importance of going beyond them. While DFT-D may yield good agreement with experiment for some MOFs, it can perform significantly worse for others. This variability highlights why consistency and reliability are just as important as accuracy when making predictions for systems lacking experimental data.

5. Conclusions

We employ the chemically accurate MP2:PBE+D4 methodology for periodic systems to investigate CO_2, N_2, and H_2 adsorption in the Zn^{2+}-containing zeolites FAU and CHA, as well as CO_2 and H_2 adsorption in the MOFs CALF-20 and Zn-MOF-74. For Zn-CHA, Zn-MOF-74, and CALF-20, our calculated CO_2 adsorption enthalpies deviate by no more than ±4 kJ mol^{-1} from experimental values, placing them within the range of chemical accuracy. This demonstrates that the approach provides reliable and consistent predictions for heats of adsorption. In addition, we provide predictions of adsorption enthalpies for CO_2 in Zn-FAU, N_2 in Zn-CHA and Zn-FAU, and H_2 in Zn-CHA, Zn-FAU, and CALF-20, for which no experimental data are currently available.

Among the tested DFT approaches, PBE+TS/HI shows the best agreement with both experiment and MP2-level results for CO_2 adsorption in Zn-CHA. However, the accuracy of DFT-D methods varies notably across systems. For example, PBE+D4 performs well for CO_2 adsorption in CALF-20 but less so for Zn-MOF-74. This inconsistency highlights the importance of high-level methods such as MP2:PBE+D4 for making accurate and reliable predictions. This is particularly important in the absence of experimental data, such as in the screening of new materials.

Our results confirm that Zn^{2+} cations are the primary CO_2 adsorption sites in zeolites, with a strong preference for incorporation into 6-membered rings. The preferred binding sites are determined by the local coordination environment of the cation rather than the positions of Al atoms in the framework. This independence from the Al positions contrasts with the behaviour observed for protons forming BASs. The preferred Zn^{2+} locations are supported by the relative stabilities of different adsorption sites, and the good agreement between calculated and experimental CO_2 adsorption enthalpies and IR spectra.

CO_2 adsorption is generally stronger than that of N_2, with both binding significantly more strongly than H_2. However, the MP2:PBE+D4 Gibbs free energies of adsorption reverse this preference in Zn-CHA, resulting in stronger N_2 adsorption. In contrast, for Zn-FAU, CO_2 adsorption remains exergonic, while adsorption of both N_2 and H_2 is endergonic. This renders Zn-FAU a particularly promising material for selective CO_2 adsorption and carbon capture applications. Moreover, both Zn-FAU and Zn-CHA exhibit CO_2 adsorption strengths that exceed those of the two MOFs by 10 to 20 kJ mol^{-1} and may therefore even represent promising competitors to industrial benchmark materials,[28,107] such as zeolite 13X.

Author contributions

P. P. Samal: writing – original draft, writing – review and editing, investigation, data curation, formal analysis, methodology, validation, visualisation. S. Krishnamurty: supervision, funding acquisition. F. Berger: conceptualisation, writing – original draft, writing – review and editing, investigation,

formal analysis, methodology, validation, supervision, funding acquisition. J. Sauer: conceptualisation, writing – review and editing, supervision, funding acquisition, project administration, resources.

Conflicts of interest

The authors declare no conflict of interest.

Data availability

The data supporting this article, including coordinates and example input files, are provided as part of the supplementary information (SI). See DOI: https://doi.org/10.1039/d5cp04169d.

Acknowledgements

This work has been funded by the Deutsche Forschungsgemeinschaft (DFG, German Research Foundation) – 509313931 and 514934444. P. P. S. and S. K. acknowledge the German Academic Exchange Service (DAAD) and HCP44-02 for providing the funding and support throughout the research work. F. B. acknowledges support from the Alexander von Humboldt Foundation through a Feodor Lynen Research Fellowship, from the Isaac Newton Trust through an Early Career Fellowship, and from Churchill College, Cambridge, through a Postdoctoral By-Fellowship.

References

1 N. Sazali, Emerging Technologies by Hydrogen: A Review, *Int. J. Hydrogen Energy*, 2020, **45**(38), 18753–18771, DOI: 10.1016/j.ijhydene.2020.05.021.
2 J.-X. Lin, W.-J. Wang, B.-Y. Yu, C. W. Ong and C.-L. Chen, Intensification of the CO_2-Capturing Methanol Steam Reforming Process: A Comprehensive Analysis of Energy, Economic and Environmental Impacts, *Sep. Purif. Technol.*, 2024, **347**, 127612, DOI: 10.1016/j.seppur.2024.127612.
3 E. J. Abraham, P. Linke, M. Al-Rawashdeh, J. Rousseau, G. Burton and D. M. Al-Mohannadi, Large-Scale Shipping of Low-Carbon Fuels and Carbon Dioxide towards Decarbonized Energy Systems: Perspectives and Challenges, *Int. J. Hydrogen Energy*, 2024, **63**, 217–230, DOI: 10.1016/j.ijhydene.2024.03.140.
4 B. M. Balasubramaniam, P.-T. Thierry, S. Lethier, V. Pugnet, P. Llewellyn and A. Rajendran, Process-Performance of Solid Sorbents for Direct Air Capture (DAC) of CO_2 in Optimized Temperature-Vacuum Swing Adsorption (TVSA) Cycles, *Chem. Eng. J.*, 2024, **485**, 149568, DOI: 10.1016/j.cej.2024.149568.
5 J. Tingelinhas, C. Saragoça, A. Al Mohtar, M. Mateus and M. L. Pinto, Pillared Clays as Cost-Effective Adsorbents for Carbon Capture by Pressure Swing Adsorption Processes in the Cement Industry, *Ind. Eng. Chem. Res.*, 2023, **62**(13), 5613–5623, DOI: 10.1021/acs.iecr.2c04209.
6 S. Chowdhury, Y. Kumar, S. Shrivastava, S. K. Patel and J. S. Sangwai, A Review on the Recent Scientific and Commercial Progress on the Direct Air Capture Technology to Manage Atmospheric CO_2 Concentrations and Future Perspectives, *Energy Fuels*, 2023, **37**(15), 10733–10757, DOI: 10.1021/acs.energyfuels.2c03971.
7 Y. Abdullatif, A. Sodiq, N. Mir, Y. Bicer, T. Al-Ansari, M. H. El-Naas and A. I. Amhamed, Emerging Trends in Direct Air Capture of CO_2: A Review of Technology Options Targeting Net-Zero Emissions, *RSC Adv.*, 2023, **13**(9), 5687–5722, DOI: 10.1039/D2RA07940B.
8 A. Rajendran, S. G. Subraveti, K. N. Pai, V. Prasad and Z. Li, How Can (or Why Should) Process Engineering Aid the Screening and Discovery of Solid Sorbents for CO_2 Capture?, *Acc. Chem. Res.*, 2023, **56**(17), 2354–2365, DOI: 10.1021/acs.accounts.3c00335.
9 P. A. Saenz Cavazos, E. Hunter-Sellars, P. Iacomi, S. R. McIntyre, D. Danaci and D. R. Williams, Evaluating Solid Sorbents for CO_2 Capture: Linking Material Properties and Process Efficiency via Adsorption Performance, *Front. Energy Res.*, 2023, **11**, 1167043, DOI: 10.3389/fenrg.2023.1167043.
10 J. S. A. Carneiro, G. Innocenti, H. J. Moon, Y. Guta, L. Proaño, C. Sievers, M. A. Sakwa-Novak, E. W. Ping and C. W. Jones, Insights into the Oxidative Degradation Mechanism of Solid Amine Sorbents for CO_2 Capture from Air: Roles of Atmospheric Water, *Angew. Chem., Int. Ed.*, 2023, **62**, e202302887, DOI: 10.1002/ange.202302887.
11 R. E. Siegel, S. Pattanayak and L. A. Berben, Reactive Capture of CO_2: Opportunities and Challenges, *ACS Catal.*, 2023, **13**(1), 766–784, DOI: 10.1021/acscatal.2c05019.
12 H. Lyu, H. Li, N. Hanikel, K. Wang and O. M. Yaghi, Covalent Organic Frameworks for Carbon Dioxide Capture from Air, *J. Am. Chem. Soc.*, 2022, **144**(28), 12989–12995, DOI: 10.1021/jacs.2c05382.
13 H. Li, A. Dilipkumar, S. Abubakar and D. Zhao, Covalent Organic Frameworks for CO_2 Capture: From Laboratory Curiosity to Industry Implementation, *Chem. Soc. Rev.*, 2023, **52**(18), 6294–6329, DOI: 10.1039/D2CS00465H.
14 P. Murge, S. Dinda and S. Roy, Zeolite-Based Sorbent for CO_2 Capture: Preparation and Performance Evaluation, *Langmuir*, 2019, **35**(46), 14751–14760, DOI: 10.1021/acs.langmuir.9b02259.
15 R. Krishna and J. M. van Baten, A Comparison of the CO_2 Capture Characteristics of Zeolites and Metal–Organic Frameworks, *Sep. Purif. Technol.*, 2012, **87**, 120–126, DOI: 10.1016/j.seppur.2011.11.031.
16 C. Lu, H. Bai, B. Wu, F. Su and J. F. Hwang, Comparative Study of CO_2 Capture by Carbon Nanotubes, Activated Carbons, and Zeolites, *Energy Fuels*, 2008, **22**(5), 3050–3056, DOI: 10.1021/ef8000086.
17 A. Hayat, S. Rauf, B. Al Alwan, A. El Jery, N. Almuqati, S. Melhi, M. A. Amin, Y. Al-Hadeethi, M. Sohail, Y. Orooji and W. Lv, Recent Advance in MOFs and MOF-Based Composites: Synthesis, Properties, and Applications, *Mater. Today Energy*, 2024, **41**, 101542, DOI: 10.1016/j.mtener.2024.101542.

18 K. Zhang and R. Wang, A Critical Review on New and Efficient Adsorbents for CO_2 Capture, *Chem. Eng. J.*, 2024, **485**, 149495, DOI: 10.1016/j.cej.2024.149495.
19 M. Younas, M. Rezakazemi, M. Daud, M. B. Wazir, S. Ahmad, N. Ullah, Inamuddin and S. Ramakrishna, Recent Progress and Remaining Challenges in Post-Combustion CO_2 Capture Using Metal–Organic Frameworks (MOFs), *Prog. Energy Combust. Sci.*, 2020, **80**, 100849, DOI: 10.1016/j.pecs.2020.100849.
20 H. Demir, G. O. Aksu, H. C. Gulbalkan and S. Keskin, MOF Membranes for CO_2 Capture: Past, Present and Future, *Carbon Capture Sci. Technol.*, 2022, **2**, 100026, DOI: 10.1016/j.ccst.2021.100026.
21 N. Jodaeeasl, S. Wang, A. Hu and G. H. Peslherbe, Comprehensive DFT Investigation of Small-Molecule Adsorption on the Paradigm M-MOF-74 Family of Metal–Organic Frameworks, *Phys. Chem. Chem. Phys.*, 2025, **27**(6), 3068–3082, DOI: 10.1039/D4CP02873B.
22 D. Adhikari, R. Karki, K. Adhikari and N. Pantha, First-Principles Study on CO, CO_2 and CH_4 Capture on Mg-MOF-74, *Phys. B*, 2025, **705**, 417071, DOI: 10.1016/J.PHYSB.2025.417071.
23 X.-Y. Yang, L.-H. Chen, Y. Li, J. C. Rooke, C. Sanchez and B.-L. Su, Hierarchically Porous Materials: Synthesis Strategies and Structure Design, *Chem. Soc. Rev.*, 2017, **46**(2), 481–558, DOI: 10.1039/C6CS00829A.
24 A. M. Najafi, S. Soltanali and H. Ghassabzadeh, Enhancing the CO_2, CH_4, and N_2 Adsorption and Kinetic Performance on FAU Zeolites for CO_2 Capture from Flue Gas by Metal Incorporation Technique, *Chem. Eng. J.*, 2023, **468**, 143719, DOI: 10.1016/j.cej.2023.143719.
25 H. Prats, D. Bahamon, G. Alonso, X. Giménez, P. Gamallo and R. Sayós, Optimal Faujasite Structures for Post Combustion CO_2 Capture and Separation in Different Swing Adsorption Processes, *J. CO2 Util.*, 2017, **19**, 100–111, DOI: 10.1016/j.jcou.2017.03.007.
26 M. Debost, P. B. Klar, N. Barrier, E. B. Clatworthy, J. Grand, F. Laine, P. Brázda, L. Palatinus, N. Nesterenko, P. Boullay and S. Mintova, Synthesis of Discrete CHA Zeolite Nanocrystals without Organic Templates for Selective CO_2 Capture, *Angew. Chem., Int. Ed.*, 2020, **59**(52), 23491–23495, DOI: 10.1002/anie.202009397.
27 S. Ghojavand, B. Coasne, E. B. Clatworthy, R. Guillet-Nicolas, P. Bazin, M. Desmurs, L. Jacobo Aguilera, V. Ruaux and S. Mintova, Alkali Metal Cations Influence the CO_2 Adsorption Capacity of Nanosized Chabazite: Modeling vs Experiment, *ACS Appl. Nano Mater.*, 2022, **5**(4), 5578–5588, DOI: 10.1021/acsanm.2c00537.
28 D. Fu, Y. Park and M. E. Davis, Zinc Containing Small-Pore Zeolites for Capture of Low Concentration Carbon Dioxide, *Angew. Chem., Int. Ed.*, 2022, **61**(5), e202112916, DOI: 10.1002/anie.202112916.
29 A. Daouli, J. Rey, E. H. Lahrar, V. Valtchev, M. Badawi and R. Guillet-Nicolas, Ab Initio Screening of Divalent Cations for CH_4, CO_2, H_2, and N_2 Separations in Chabazite Zeolite, *Langmuir*, 2023, **39**(45), 15962–15973, DOI: 10.1021/acs.langmuir.3c01882.
30 J.-B. Lin, T. T. T. Nguyen, R. Vaidhyanathan, J. Burner, J. M. Taylor, H. Durekova, F. Akhtar, R. K. Mah, O. Ghaffari-Nik, S. Marx, N. Fylstra, S. S. Iremonger, K. W. Dawson, P. Sarkar, P. Hovington, A. Rajendran, T. K. Woo and G. K. H. Shimizu, A Scalable Metal–Organic Framework as a Durable Physisorbent for Carbon Dioxide Capture, *Science*, 2021, **374**(6574), 1464–1469, DOI: 10.1126/science.abi7281.
31 S. Chatterjee, S. Jeevanandham, M. Mukherjee, D.-V. N. Vo and V. Mishra, Significance of Re-Engineered Zeolites in Climate Mitigation – A Review for Carbon Capture and Separation, *J. Environ. Chem. Eng.*, 2021, **9**(5), 105957, DOI: 10.1016/j.jece.2021.105957.
32 M. Pera-Titus, Porous Inorganic Membranes for CO_2 Capture: Present and Prospects, *Chem. Rev.*, 2014, **114**(2), 1413–1492, DOI: 10.1021/cr400237k.
33 D. Fu and M. E. Davis, Carbon Dioxide Capture with Zeotype Materials, *Chem. Soc. Rev.*, 2022, **51**(22), 9340–9370, DOI: 10.1039/D2CS00508E.
34 J. Yu, L.-H. Xie, J.-R. Li, Y. Ma, J. M. Seminario and P. B. Balbuena, CO_2 Capture and Separations Using MOFs: Computational and Experimental Studies, *Chem. Rev.*, 2017, **117**(14), 9674–9754, DOI: 10.1021/acs.chemrev.6b00626.
35 Ankit, N. Saini, H. Pandey and K. Pandey, A Systematic Review of MOF, COF, and Their Hybrid-Based Composite Membranes for Gas Separation, *Macromol. Symp.*, 2024, **413**(1), 2300058, DOI: 10.1002/masy.202300058.
36 G. Singh, J. Lee, A. Karakoti, R. Bahadur, J. Yi, D. Zhao, K. AlBahily and A. Vinu, Emerging Trends in Porous Materials for CO_2 Capture and Conversion, *Chem. Soc. Rev.*, 2020, **49**(13), 4360–4404, DOI: 10.1039/D0CS00075B.
37 T. L. Easun, F. Moreau, Y. Yan, S. Yang and M. Schröder, Structural and Dynamic Studies of Substrate Binding in Porous Metal–Organic Frameworks, *Chem. Soc. Rev.*, 2017, **46**(1), 239–274, DOI: 10.1039/C6CS00603E.
38 G. Piccini, M. Alessio, J. Sauer, Y. Zhi, Y. Liu, R. Kolvenbach, A. Jentys and J. A. Lercher, Accurate Adsorption Thermodynamics of Small Alkanes in Zeolites. Ab Initio Theory and Experiment for H-Chabazite, *J. Phys. Chem. C*, 2015, **119**(11), 6128–6137, DOI: 10.1021/ACS.JPCC.5B01739/SUPPL_FILE/JP5B01739_SI_001.PDF.
39 T. Kerber, M. Sierka and J. Sauer, Application of Semiempirical Long-range Dispersion Corrections to Periodic Systems in Density Functional Theory, *J. Comput. Chem.*, 2008, **29**(13), 2088–2097, DOI: 10.1002/jcc.21069.
40 M. Alessio, D. Usvyat and J. Sauer, Chemically Accurate Adsorption Energies: CO and H_2O on the MgO(001) Surface, *J. Chem. Theory Comput.*, 2019, **15**(2), 1329–1344, DOI: 10.1021/acs.jctc.8b01122.
41 C. Tuma and J. Sauer, A Hybrid MP2/Planewave-DFT Scheme for Large Chemical Systems: Proton Jumps in Zeolites, *Chem. Phys. Lett.*, 2004, **387**(4–6), 388–394, DOI: 10.1016/j.cplett.2004.02.056.
42 C. Tuma and J. Sauer, Treating Dispersion Effects in Extended Systems by Hybrid MP2:DFT Calculations—Protonation of

Isobutene in Zeolite Ferrierite, *Phys. Chem. Chem. Phys.*, 2006, **8**(34), 3955–3965, DOI: 10.1039/B608262A.
43 S. Tosoni and J. Sauer, Accurate Quantum Chemical Energies for the Interaction of Hydrocarbons with Oxide Surfaces: CH_4/MgO(001), *Phys. Chem. Chem. Phys.*, 2010, **12**(42), 14330, DOI: 10.1039/c0cp01261k.
44 J. P. Perdew, K. Burke and M. Ernzerhof, Generalized Gradient Approximation Made Simple [Phys. Rev. Lett. 77, 3865 (1996)], *Phys. Rev. Lett.*, 1997, **78**(7), 1396, DOI: 10.1103/PhysRevLett.78.1396.
45 J. P. Perdew, K. Burke and M. Ernzerhof, Generalized Gradient Approximation Made Simple, *Phys. Rev. Lett.*, 1996, **77**(18), 3865–3868, DOI: 10.1103/PhysRevLett.77.3865.
46 S. Grimme, Semiempirical GGA-type Density Functional Constructed with a Long-range Dispersion Correction, *J. Comput. Chem.*, 2006, **27**(15), 1787–1799, DOI: 10.1002/jcc.20495.
47 E. Caldeweyher, J.-M. Mewes, S. Ehlert and S. Grimme, Extension and Evaluation of the D4 London-Dispersion Model for Periodic Systems, *Phys. Chem. Chem. Phys.*, 2020, **22**(16), 8499–8512, DOI: 10.1039/D0CP00502A.
48 D. Yu, A. O. Yazaydin, J. R. Lane, P. D. C. Dietzel and R. Q. Snurr, A Combined Experimental and Quantum Chemical Study of CO_2 Adsorption in the Metal–Organic Framework CPO-27 with Different Metals, *Chem. Sci.*, 2013, **4**(9), 3544, DOI: 10.1039/c3sc51319j.
49 K. Sumida, D. L. Rogow, J. A. Mason, T. M. McDonald, E. D. Bloch, Z. R. Herm, T.-H. Bae and J. R. Long, Carbon Dioxide Capture in Metal–Organic Frameworks, *Chem. Rev.*, 2012, **112**(2), 724–781, DOI: 10.1021/cr2003272.
50 M. Y. Borzehandani, M. N. Jorabchi, E. Abdulmalek, M. B. Abdul Rahman and M. A. Mohammad Latif, Exploring the Potential of a Highly Scalable Metal–Organic Framework CALF-20 for Selective Gas Adsorption at Low Pressure, *Polymers*, 2023, **15**(3), 760, DOI: 10.3390/polym15030760.
51 R. Oktavian, R. Goeminne, L. T. Glasby, P. Song, R. Huynh, O. T. Qazvini, O. Ghaffari-Nik, N. Masoumifard, J. L. Cordiner, P. Hovington, V. Van Speybroeck and P. Z. Moghadam, Gas Adsorption and Framework Flexibility of CALF-20 Explored via Experiments and Simulations, *Nat. Commun.*, 2024, **15**(1), 3898, DOI: 10.1038/s41467-024-48136-0.
52 J. Zhao, K. Xie, R. Singh, G. Xiao, Q. Gu, Q. Zhao, G. Li, P. Xiao and P. A. Webley, Li +/ZSM-25 Zeolite as a CO_2 Capture Adsorbent with High Selectivity and Improved Adsorption Kinetics, Showing CO_2-Induced Framework Expansion, *J. Phys. Chem. C*, 2018, **122**(33), 18933–18941, DOI: 10.1021/ACS.JPCC.8B04152/ASSET/IMAGES/LARGE/JP-2018-04152W_0007.JPEG.
53 H. Zhang, Z. Li, J. Wang, C. Wang, J. Dong, G. Liu, S. Gong, L. Shi, R. Dong and X. Huang, Integrating Four-, Five- and Six-Coordinated Zn Catalytic Centers in an Ionic-Type Zinc Catalyst for the Coupling of CO_2 with Epoxides, *J. CO2 Util.*, 2024, **82**, 102760, DOI: 10.1016/J.JCOU.2024.102760.
54 L. Benco, T. Bucko, J. Hafner and H. Toulhoat, Periodic DFT Calculations of the Stability of Al/Si Substitutions and Extraframework Zn^{2+} Cations in Mordenite and Reaction Pathway for the Dissociation of H_2 and CH_4, *J. Phys. Chem. B*, 2005, **109**(43), 20361–20369, DOI: 10.1021/JP0530597/ASSET/IMAGES/LARGE/JP0530597F00011.JPEG.
55 R. Vismara, G. Tuci, A. Tombesi, K. V. Domasevitch, C. Di Nicola, G. Giambastiani, M. R. Chierotti, S. Bordignon, R. Gobetto, C. Pettinari, A. Rossin and S. Galli, Tuning Carbon Dioxide Adsorption Affinity of Zinc(II) MOFs by Mixing Bis(Pyrazolate) Ligands with N-Containing Tags, *ACS Appl. Mater. Interfaces*, 2019, **11**(30), 26956–26969, DOI: 10.1021/acsami.9b08015.
56 A. M. Wright, Z. Wu, G. Zhang, J. L. Mancuso, R. J. Comito, R. W. Day, C. H. Hendon, J. T. Miller and M. Dincă, A Structural Mimic of Carbonic Anhydrase in a Metal–Organic Framework, *Chem*, 2018, **4**(12), 2894–2901, DOI: 10.1016/j.chempr.2018.09.011.
57 C. Baerlocher, D. Brouwer, B. Marler and L. B. McCusker, *Database of Zeolite Structures; Structure Commission of the International Zeolite Association*, 2017.
58 W. Loewenstein, The Distribution of Aluminum in the Tetrahedra of Silicates and Aluminates, *Am. Mineral.*, 1954, **39**(1–2), 92–96.
59 Y. Gao, J. Wang, C.-F. Zhang, X.-H. Xu, M. Zhang and L.-Y. Kong, *Experimental Crystal Structure Determination*, Cambridge Crystallographic Data Centre. 2014.
60 H. Neugebauer, P. Pinski, S. Grimme, F. Neese and M. Bursch, Assessment of DLPNO-MP2 Approximations in Double-Hybrid DFT, *J. Chem. Theory Comput.*, 2023, **19**(21), 7695–7703, DOI: 10.1021/acs.jctc.3c00896.
61 F. Berger, M. Rybicki and J. Sauer, Molecular Dynamics with Chemical Accuracy—Alkane Adsorption in Acidic Zeolites, *ACS Catal.*, 2023, **13**(3), 2011–2024, DOI: 10.1021/acscatal.2c05493.
62 H. Windeck, F. Berger and J. Sauer, Chemically Accurate Predictions for Water Adsorption on Brønsted Sites of Zeolite H-MFI, *Phys. Chem. Chem. Phys.*, 2024, **26**, 23588, DOI: 10.1039/D4CP02851A.
63 F. Berger and J. Sauer, Dimerization of Linear Butenes and Pentenes in an Acidic Zeolite (H-MFI), *Angew. Chem., Int. Ed.*, 2021, **60**(7), 3529–3533, DOI: 10.1002/ANIE.202013671.
64 F. Berger, M. Rybicki and J. Sauer, Adsorption and Cracking of Propane by Zeolites of Different Pore Size, *J. Catal.*, 2021, **395**, 117–128, DOI: 10.1016/J.JCAT.2020.12.008.
65 G. Kresse and J. Furthmüller, Efficient Iterative Schemes for Ab Initio Total-Energy Calculations Using a Plane-Wave Basis Set, *Phys. Rev. B: Condens. Matter Mater. Phys.*, 1996, **54**(16), 11169–11186, DOI: 10.1103/PhysRevB.54.11169.
66 G. Kresse and J. Furthmüller, Efficient Iterative Schemes for Ab Initio Total-Energy Calculations Using a Plane-Wave Basis Set, *Phys. Rev. B: Condens. Matter Mater. Phys.*, 1996, **54**(16), 11169–11186, DOI: 10.1103/PhysRevB.54.11169.
67 G. Kresse and D. Joubert, From Ultrasoft Pseudopotentials to the Projector Augmented-Wave Method, *Phys. Rev. B: Condens. Matter Mater. Phys.*, 1999, **59**(3), 1758–1775, DOI: 10.1103/PhysRevB.59.1758.

68 F. A. Bischoff, M. Alessio, F. Berger, M. John, M. Rybicki and J. Sauer, *Multi-Level Energy Landscapes: The MonaLisa Program*, Humboldt-University, Berlin, 2019.
69 M. Alessio, D. Usvyat and J. Sauer, Chemically Accurate Adsorption Energies: CO and H_2O on the MgO(001) Surface, *J. Chem. Theory Comput.*, 2019, **15**(2), 1329–1344, DOI: 10.1021/acs.jctc.8b01122.
70 Chr Møller and M. S. Plesset, Note on an Approximation Treatment for Many-Electron Systems, *Phys. Rev.*, 1934, **46**(7), 618–622, DOI: 10.1103/PhysRev.46.618.
71 S. F. Boys and F. Bernardi, The Calculation of Small Molecular Interactions by the Differences of Separate Total Energies. Some Procedures with Reduced Errors, *Mol. Phys.*, 1970, **19**(4), 553–566, DOI: 10.1080/00268977000101561.
72 F. Neese, The ORCA Program System, *Wiley Interdiscip. Rev.: Comput. Mol. Sci.*, 2012, **2**(1), 73–78, DOI: 10.1002/wcms.81.
73 F. Neese, Software Update: The ORCA Program System, Version 4.0, *Wiley Interdiscip. Rev.: Comput. Mol. Sci.*, 2018, **8**(1), e1327, DOI: 10.1002/wcms.1327.
74 F. Neese, F. Wennmohs, U. Becker and C. Riplinger, The ORCA Quantum Chemistry Program Package, *J. Chem. Phys.*, 2020, **152**(22), 224108, DOI: 10.1063/5.0004608.
75 F. Weigend and R. Ahlrichs, Balanced Basis Sets of Split Valence, Triple Zeta Valence and Quadruple Zeta Valence Quality for H to Rn: Design and Assessment of Accuracy, *Phys. Chem. Chem. Phys.*, 2005, **7**(18), 3297, DOI: 10.1039/b508541a.
76 F. Weigend, M. Häser, H. Patzelt and R. Ahlrichs, RI-MP2: Optimized Auxiliary Basis Sets and Demonstration of Efficiency, *Chem. Phys. Lett.*, 1998, **294**(1–3), 143–152, DOI: 10.1016/S0009-2614(98)00862-8.
77 S. Svelle, C. Tuma, X. Rozanska, T. Kerber and J. Sauer, Quantum Chemical Modeling of Zeolite-Catalyzed Methylation Reactions: Toward Chemical Accuracy for Barriers, *J. Am. Chem. Soc.*, 2009, **131**(2), 816–825, DOI: 10.1021/ja807695p.
78 P. Pinski, C. Riplinger, E. F. Valeev and F. Neese, Sparse Maps—A Systematic Infrastructure for Reduced-Scaling Electronic Structure Methods. I. An Efficient and Simple Linear Scaling Local MP2 Method That Uses an Intermediate Basis of Pair Natural Orbitals, *J. Chem. Phys.*, 2015, **143**(3), 034108, DOI: 10.1063/1.4926879.
79 C. Riplinger, P. Pinski, U. Becker, E. F. Valeev and F. Neese, Sparse Maps—A Systematic Infrastructure for Reduced-Scaling Electronic Structure Methods. II. Linear Scaling Domain Based Pair Natural Orbital Coupled Cluster Theory, *J. Chem. Phys.*, 2016, **144**(2), 024109, DOI: 10.1063/1.4939030.
80 A. Karton and J. M. L. Martin, Comment on: "Estimating the Hartree–Fock Limit from Finite Basis Set Calculations" [Jensen F (2005) Theor Chem Acc 113:267], *Theor. Chem. Acc.*, 2006, **115**(4), 330–333, DOI: 10.1007/s00214-005-0028-6.
81 T. Helgaker, W. Klopper, H. Koch and J. Noga, Basis-Set Convergence of Correlated Calculations on Water, *J. Chem. Phys.*, 1997, **106**(23), 9639–9646, DOI: 10.1063/1.473863.
82 T. H. Dunning, Gaussian Basis Sets for Use in Correlated Molecular Calculations. I. The Atoms Boron through Neon and Hydrogen, *J. Chem. Phys.*, 1989, **90**(2), 1007–1023, DOI: 10.1063/1.456153.
83 D. E. Woon and T. H. Dunning, Gaussian Basis Sets for Use in Correlated Molecular Calculations. III. The Atoms Aluminum through Argon, *J. Chem. Phys.*, 1993, **98**(2), 1358–1371, DOI: 10.1063/1.464303.
84 C. Tuma and J. Sauer, Quantum Chemical Ab Initio Prediction of Proton Exchange Barriers between CH_4 and Different H-Zeolites, *J. Chem. Phys.*, 2015, **143**(10), 102810, DOI: 10.1063/1.4923086.
85 F. Berger, J. Schumann, R. Réocreux, M. Stamatakis and A. Michaelides, Bringing Molecules Together: Synergistic Coadsorption at Dopant Sites of Single Atom Alloys, *J. Am. Chem. Soc.*, 2024, **146**, 28119, DOI: 10.1021/jacs.4c07621.
86 T. Bučko, S. Lebègue, J. Hafner and J. G. Ángyán, Tkatchenko-Scheffler van der Waals Correction Method with and without Self-Consistent Screening Applied to Solids, *Phys. Rev. B: Condens. Matter Mater. Phys.*, 2013, **87**(6), 064110, DOI: 10.1103/PhysRevB.87.064110.
87 A. Tkatchenko and M. Scheffler, Accurate Molecular van der Waals Interactions from Ground-State Electron Density and Free-Atom Reference Data, *Phys. Rev. Lett.*, 2009, **102**(7), 073005, DOI: 10.1103/PhysRevLett.102.073005.
88 T. Bučko, S. Lebègue, J. Hafner and J. G. Ángyán, Improved Density Dependent Correction for the Description of London Dispersion Forces, *J. Chem. Theory Comput.*, 2013, **9**(10), 4293–4299, DOI: 10.1021/ct400694h.
89 A. Tkatchenko, R. A. DiStasio, R. Car and M. Scheffler, Accurate and Efficient Method for Many-Body van der Waals Interactions, *Phys. Rev. Lett.*, 2012, **108**(23), 236402, DOI: 10.1103/PhysRevLett.108.236402.
90 M. Á. Hernández, K. Quiroz-Estrada, G. I. Hernandez-Salgado, R. I. Portillo, J. D. Santamaría-Juárez, M. D. L. Á. Velasco, E. Rubio and V. Petranovskii, Nanoporosity and Isosteric Enthalpy of Adsorption of CH_4, H_2, and CO_2 on Natural Chabazite and Exchanged, *Separations*, 2022, **9**(6), 150, DOI: 10.3390/separations9060150.
91 T. D. Pham, M. R. Hudson, C. M. Brown and R. F. Lobo, Molecular Basis for the High CO_2 Adsorption Capacity of Chabazite Zeolites, *ChemSusChem*, 2014, **7**(11), 3031–3038, DOI: 10.1002/cssc.201402555.
92 G. Avci, I. Erucar and S. Keskin, Do New MOFs Perform Better for CO_2 Capture and H_2 Purification? Computational Screening of the Updated MOF Database, *ACS Appl. Mater. Interfaces*, 2020, **12**(37), 41567–41579, DOI: 10.1021/acsami.0c12330.
93 G. Avci, S. Velioglu and S. Keskin, High-Throughput Screening of MOF Adsorbents and Membranes for H_2 Purification and CO_2 Capture, *ACS Appl. Mater. Interfaces*, 2018, **10**(39), 33693–33706, DOI: 10.1021/acsami.8b12746.
94 T. T. T. Nguyen, J.-B. Lin, G. K. H. Shimizu and A. Rajendran, Separation of CO_2 and N_2 on a Hydrophobic Metal Organic Framework CALF-20, *Chem. Eng. J.*, 2022, **442**, 136263, DOI: 10.1016/j.cej.2022.136263.

95 R. Oktavian, R. Goeminne, L. T. Glasby, P. Song, R. Huynh, O. T. Qazvini, O. Ghaffari-Nik, N. Masoumifard, J. L. Cordiner, P. Hovington, V. Van Speybroeck and P. Z. Moghadam, Gas Adsorption and Framework Flexibility of CALF-20 Explored via Experiments and Simulations, *Nat. Commun.*, 2024, **15**(1), 3898, DOI: 10.1038/s41467-024-48136-0.

96 N. Vrtovec, S. Jurjevec, N. Zabukovec Logar, M. Mazaj and S. Kovačič, Metal Oxide-Derived MOF-74 Polymer Composites through Pickering Emulsion-Templating: Interfacial Recrystallization, Hierarchical Architectures, and CO_2 Capture Performances, *ACS Appl. Mater. Interfaces*, 2023, **15**(14), 18354–18361, DOI: 10.1021/acsami.3c01796.

97 D.-A. Yang, H.-Y. Cho, J. Kim, S.-T. Yang and W.-S. Ahn, CO_2 Capture and Conversion Using Mg-MOF-74 Prepared by a Sonochemical Method, *Energy Environ. Sci.*, 2012, **5**(4), 6465–6473, DOI: 10.1039/C1EE02234B.

98 J. Yu and P. B. Balbuena, Water Effects on Postcombustion CO_2 Capture in Mg-MOF-74, *J. Phys. Chem. C*, 2013, **117**(7), 3383–3388, DOI: 10.1021/jp311118x.

99 J. H. Choe, H. Kim and C. S. Hong, MOF-74 Type Variants for CO_2 Capture, *Mater. Chem. Front.*, 2021, **5**(14), 5172–5185, DOI: 10.1039/D1QM00205H.

100 L. Valenzano, B. Civalleri, K. Sillar and J. Sauer, Heats of Adsorption of CO and CO_2 in Metal–Organic Frameworks: Quantum Mechanical Study of CPO-27-M (M = Mg, Ni, Zn), *J. Phys. Chem. C*, 2011, **115**(44), 21777–21784, DOI: 10.1021/jp205869k.

101 K. Lee, J. D. Howe, L.-C. Lin, B. Smit and J. B. Neaton, Small-Molecule Adsorption in Open-Site Metal–Organic Frameworks: A Systematic Density Functional Theory Study for Rational Design, *Chem. Mater.*, 2015, **27**(3), 668–678, DOI: 10.1021/cm502760q.

102 T. Pham, K. A. Forrest, R. Banerjee, G. Orcajo, J. Eckert and B. Space, Understanding the H_2 Sorption Trends in the M-MOF-74 Series (M = Mg, Ni, Co, Zn), *J. Phys. Chem. C*, 2015, **119**(2), 1078–1090, DOI: 10.1021/jp510253m.

103 A. K. Adhikari and K.-S. Lin, Synthesis, Fine Structural Characterization, and CO_2 Adsorption Capacity of Metal Organic Frameworks-74, *J. Nanosci. Nanotechnol.*, 2014, **14**(4), 2709–2717, DOI: 10.1166/jnn.2014.8621.

104 X. Li, W. Shen, H. Sun, L. Meng, B. Wang, C. Zhan and B. Zhao, Theoretical Studies on Carbon Dioxide Adsorption in Cation-Exchanged Molecular Sieves, *RSC Adv.*, 2020, **10**(53), 32241–32248, DOI: 10.1039/D0RA05228K.

105 D. G. Boer, J. Langerak and P. P. Pescarmona, Zeolites as Selective Adsorbents for CO_2 Separation, *ACS Appl. Energy Mater.*, 2023, **6**(5), 2634–2656, DOI: 10.1021/acsaem.2c03605.

106 M. Polisi, J. Grand, R. Arletti, N. Barrier, S. Komaty, M. Zaarour, S. Mintova and G. Vezzalini, CO_2 Adsorption/Desorption in FAU Zeolite Nanocrystals: In Situ Synchrotron X-Ray Powder Diffraction and in Situ Fourier Transform Infrared Spectroscopic Study, *J. Phys. Chem. C*, 2019, **123**(4), 2361–2369, DOI: 10.1021/acs.jpcc.8b11811.

107 K. N. Son, G. E. Cmarik, J. C. Knox, J. A. Weibel and S. V. Garimella, Measurement and Prediction of the Heat of Adsorption and Equilibrium Concentration of CO_2 on Zeolite 13X, *J. Chem. Eng. Data*, 2018, **63**(5), 1663–1674, DOI: 10.1021/acs.jced.8b00019.

